Supporting Information

Zinc(II)-based coordination polymer encapsulated by Tb^{3+} as multiresponsive luminescent sensor for Ru^{3+}, Fe^{3+}, CrO_4^{2-}, $Cr_2O_7^{2-}$ and MnO_4^-

Yuandi Wu,[a] Dongyang Liu,[a] Meihua Lin,[a] Jing Qian,[a*,b,c]

Corresponding authors: a* qianjinger@aliyun.com (J. Qian)

a *College of Chemistry, Tianjin Normal University, Tianjin 300387, P. R. China*

b *Tianjin Key Laboratory of Structure and Performance for Functional Molecules, Tianjin Normal University, Tianjin 300387, P. R. China*

c *Key Laboratory of Inorganic−Organic Hybrid Functional Materials Chemistry, Tianjin Normal University, Ministry of Education, Tianjin 300387, P. R. China*

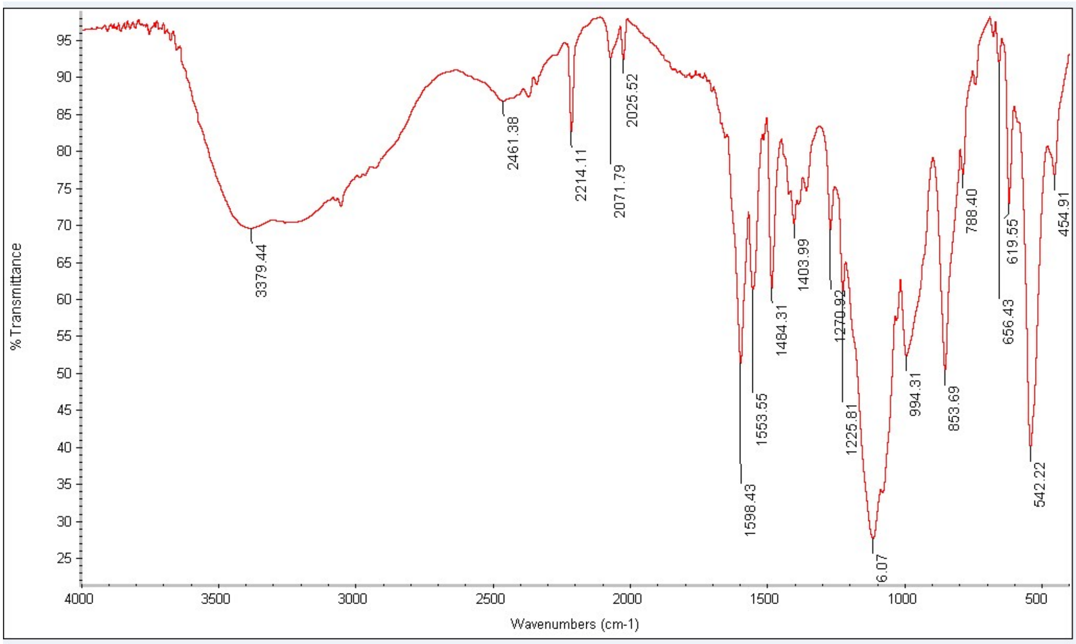

Fig. S1 FTIR pattern for Zn-CP.

Table S1 Crystal data and structure refinement information for Zn-CP

polymer	Zn-CP
CCDC	1882227
Formula	$C_{3.43}H_{2.29}N_{0.86}O_{0.29}Zn_{0.14}$
fw	69.40
temp (K)	296(2)
cryst syst	Tetragonal
Space group	$P4_32_12$
a(Å)	10.4340(10)
b(Å)	10.4340(10)
c(Å)	20.752(5)
$\alpha = \beta = \gamma$(°)	90
V (A^3)	2259.2(7)
Z	28
ρ (Mg/m^3)	1.428
Abs coeff (mm^{-1})	1.120
F (000)	992
GOF	0.924

R_1/wR_2 [I >2σ(I)]	0.0310/0.0687
R_1/wR_2 (all data)	0.0406/0.0730

Table S2 Selected bond lengths (A˚) and angles (◦) for Zn-CP

Bond lengths (Å)			
Zn(1)-N(2)#1	2.089(2)	Zn(1)-N(2)#2	2.089(2)
Zn(1)-N(1)#3	2.104(2)	Zn(1)-N(1)	2.104(2)
Zn(1)-O(1)	2.390(2)	Zn(1)-O(1)#3	2.390(2)
N(2)-Zn(1)#4	2.089(2)		
Bond angles (º)			
N(2)#1-Zn(1)-N(2)#2	96.22(14)	N(2)#1-Zn(1)-N(1)#3	142.64(9)
N(2)#2-Zn(1)-N(1)#3	94.05(11)	N(2)#1-Zn(1)-N(1)	94.05(11)
N(2)#2-Zn(1)-N(1)	142.64(9)	N(1)#3-Zn(1)-N(1)	99.21(14)
N(2)#1-Zn(1)-O(1)	91.01(9)	N(2)#2-Zn(1)-O(1)	84.85(8)
N(1)#3-Zn(1)-O(1)	125.70(9)	N(1)-Zn(1)-O(1)	59.10(8)
N(2)#1-Zn(1)-O(1)#3	84.85(8)	N(2)#2-Zn(1)-O(1)#3	91.01(9)
N(1)#3-Zn(1)-O(1)#3	59.10(8)	N(1)-Zn(1)-O(1)#3	125.69(9)
O(1)-Zn(1)-O(1)#3	173.81(11)		

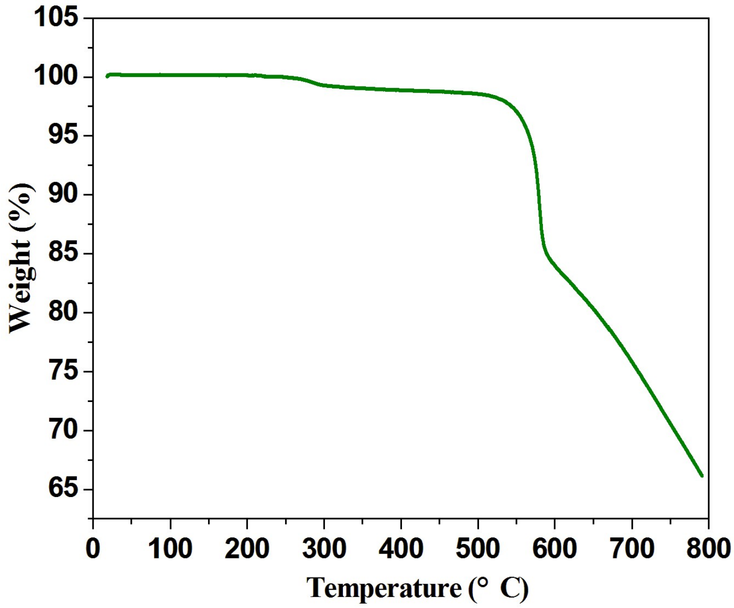

Fig. S2 Thermogravimetric curve of Zn-CP.

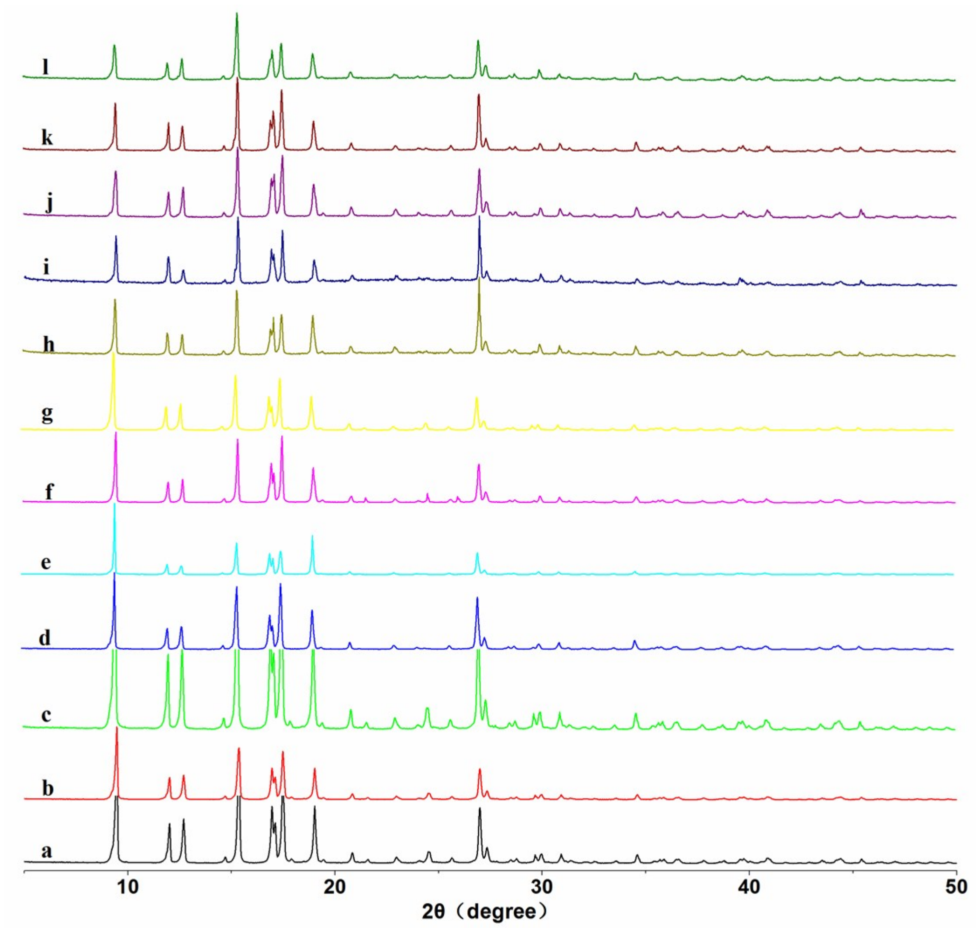

Fig. S3 PXRD patterns for Zn-CP: (a) simulated; (b) experimental; (c) 1 days after immersion in water; (d) 1 days after immersion in $FeCl_3$ solution (e) 1 days after immersion in $CoCl_2$ solution; (f) 1 days after immersion in $NiCl_2$

solution; (g) 1 days after immersion in $CuCl_2$ solution; (h) 12 h after immersion in CH_3OH; (i) 12 h after immersion in C_2H_5OH; (j) 12 h after immersion in acetone; (k) 12 h after immersion in CH_2Cl_2; (l) 12 h after immersion in DMF. PXRD pattern calculated from the single-crystal structure.

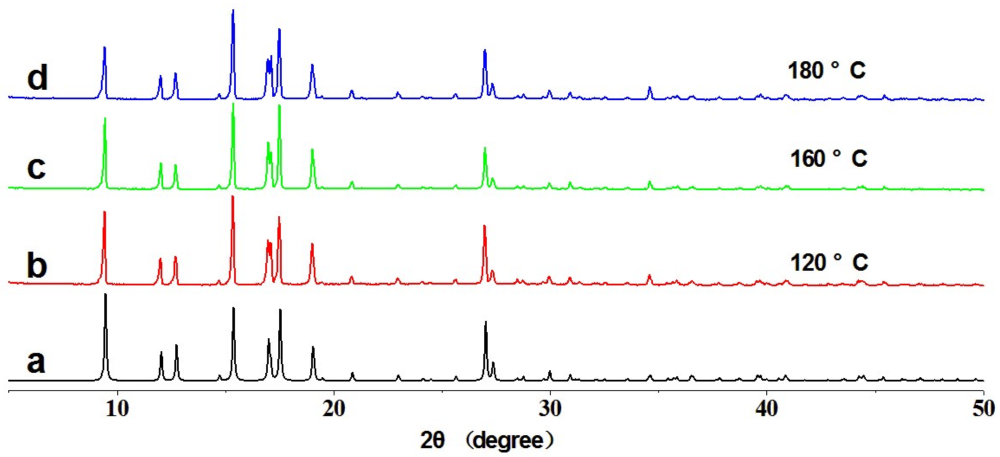

Fig. S4 PXRD patterns for Zn-CP at different temperatures, 120℃ (red line); 160℃ (green line); 180℃ (blue line) and the simulated one calculated from the single crystal structure analysis (black line).

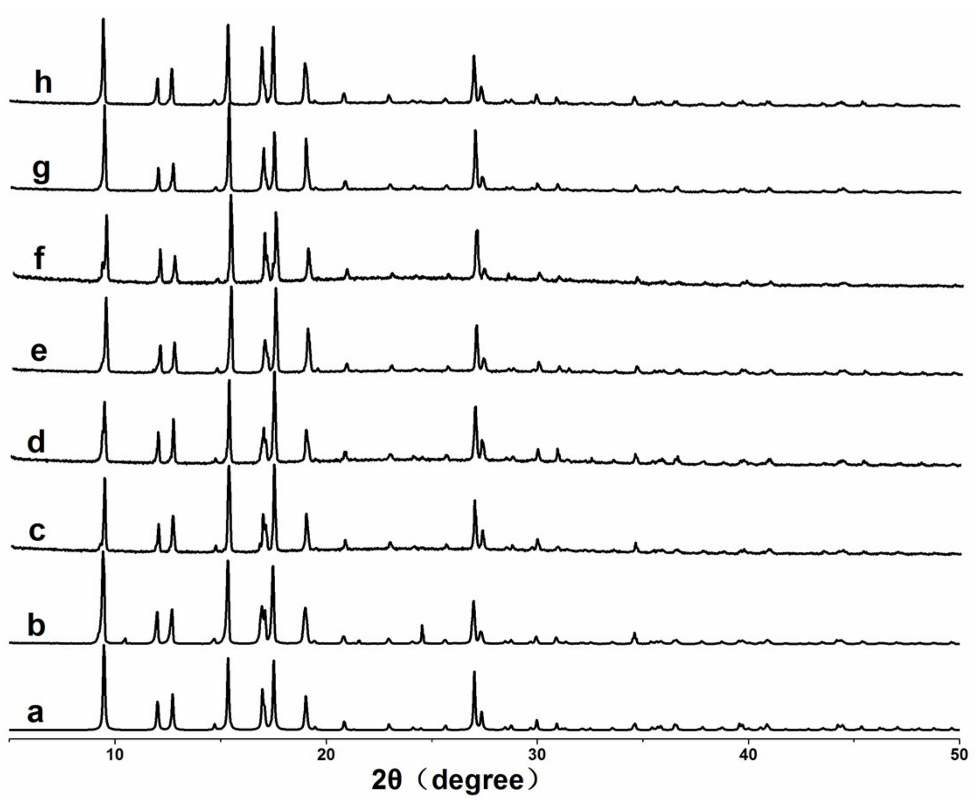

Fig. S5 PXRD patterns for Tb^{3+}@Zn-CP: (a) simulated of Zn-CP; (b) experimental of Zn-CP; (c) experimental of

Tb^{3+}@Zn-CP; (d) experimental of Tb^{3+}@Zn-CP 12 h after immersion in $FeCl_3$ solution; (e) experimental of Tb^{3+}@Zn-CP 12 h after immersion in $RuCl_3$ solution; (f) experimental of Tb^{3+}@Zn-CP 12 h after immersion in $KMnO_4$ solution; (g) experimental of Tb^{3+}@Zn-CP 12 h after immersion in K_2CrO_4 solution; (h) experimental of Tb^{3+}@Zn-CP 12 h after immersion in $K_2Cr_2O_7$ solution.

Table S3 The detailed ICP studies of Tb^{3+}@Zn-CP.

Sample	Zn(ppm)	Tb(ppm)	Mn(ppm)	Ru(ppm)	Cr(ppm)	Fe(ppm)
Tb^{3+}@Zn-CP	1.312	0.0398				
Tb^{3+}@Zn-CP+Fe^{3+}	2.897	0.0239				0.1017
Tb^{3+}@Zn-CP+Ru^{3+}	1.093	Below detection limit		Below detection limit		
Tb^{3+}@Zn-CP+MnO_4^-	2.354	0.0530	0.2275			
Tb^{3+}@Zn-CP+CrO_4^{2-}	2.747	0.0150			Below detection limit	
Tb^{3+}@Zn-CP+$Cr_2O_7^{2-}$	2.509	0.0171			Below detection limit	
detection limit/ ppm		0.007		0.003	0.002	

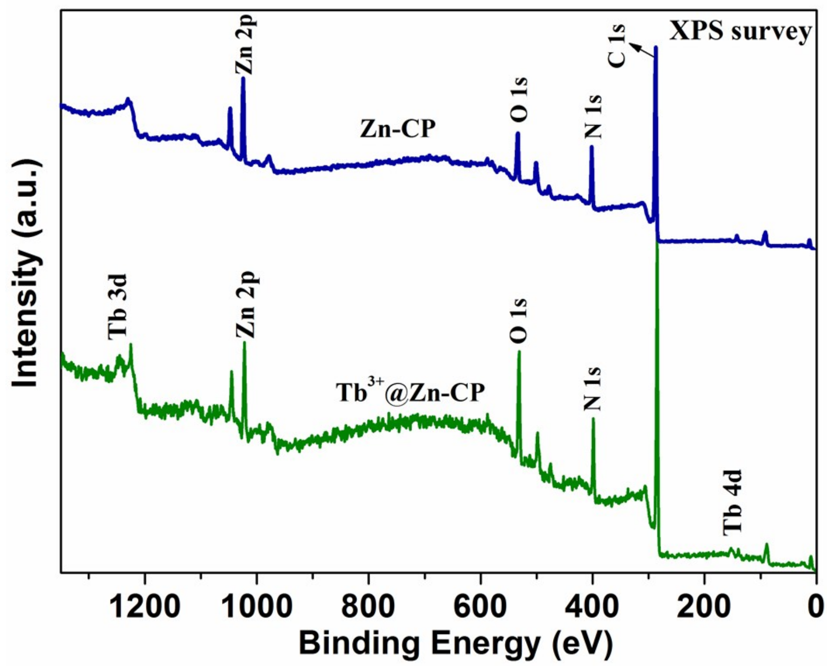

(a)

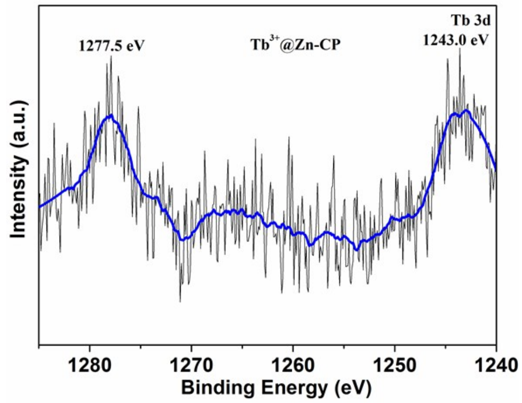

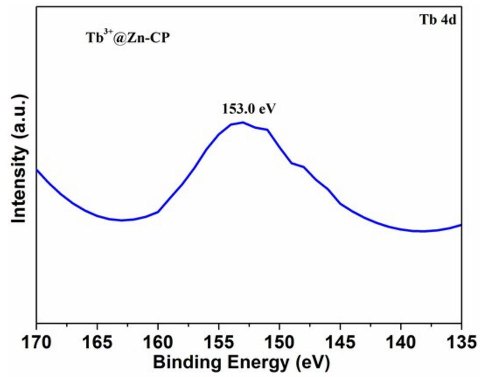

(b) **(c)**

Fig. S6 The XPS spectra of Zn-CP and Tb^{3+}@Zn-CP samples: (a) the survey spectrum, the high resolution XPS spectra of (b) Tb 3d, (c) Tb 4d, respectively.

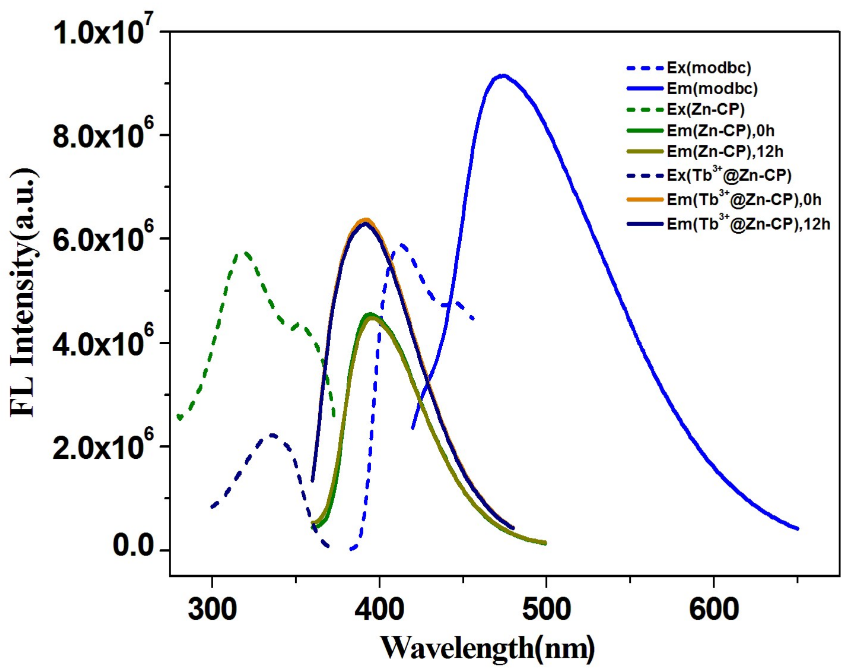

Fig. S7 liquid-state luminescent spectra of modbc ligand (blue), Zn-CP (green) , Tb^{3+}@Zn-CP (orange and navy) in 5 mM Tris-HCl/NaCl buffer (pH 7.0). slit width: 4 nm.

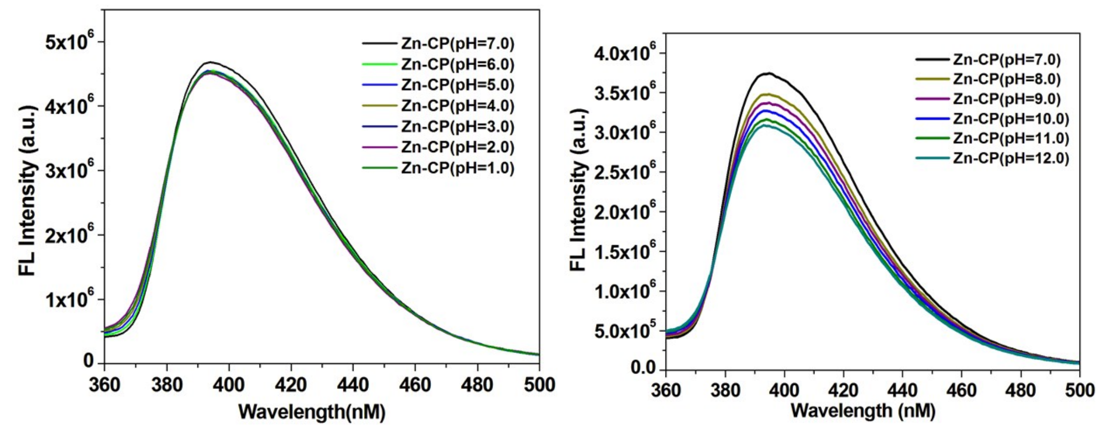

(a)

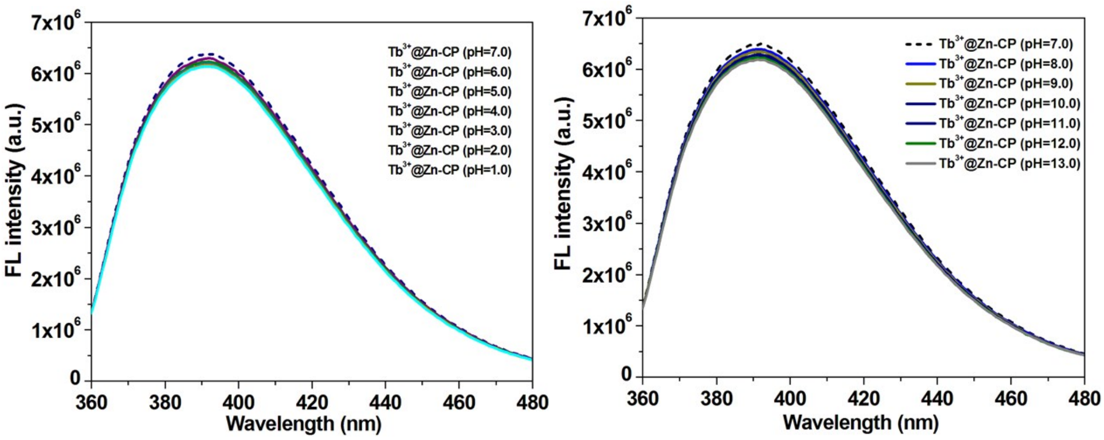

(b)

Fig. S8 Liquid-state luminescent spectra of Zn-CP upon excitation at about 312 nm (a) and Tb^{3+}@Zn-CP upon excitation at about 330 nm (b) with different pH values (1.0~13.0) in H_2O.

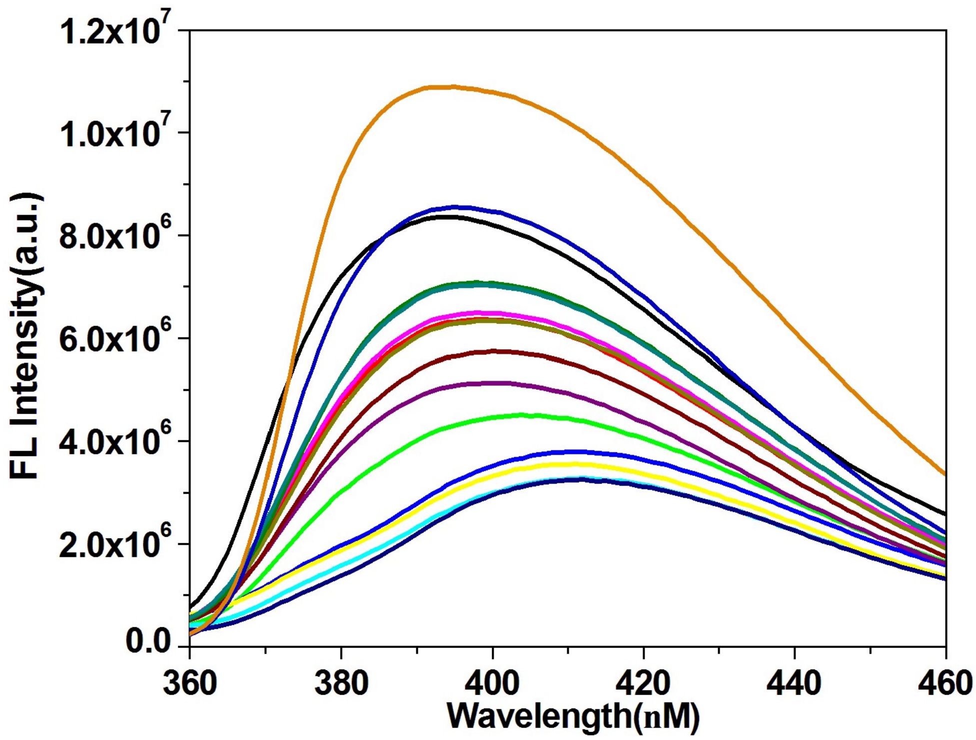

Fig. S9 Luminous intensity of Zn-CP upon different ions (Ru^{3+}, Ag^{+}, Cd^{2+}, Zn^{2+}, Pb^{2+}, Ca^{2+}, Mn^{2+}, Cu^{2+}, Co^{2+}, Ni^{2+}, Fe^{2+}, Hg^{2+} and Fe^{3+}) in 5 mM Tris-HCl/NaCl buffer (pH 7.0). [Zn-CP] = 10 μM and [ions] = 50 μM. λ_{ex}: 312 nm, λ_{F}: 395 nm, slit width: 4 nm.

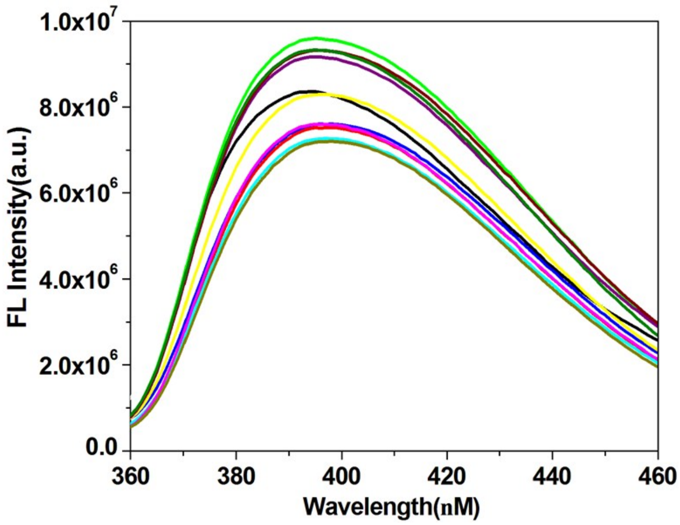

Fig. S10 Luminous intensity of Zn-CP upon different ions (SO_4^{2-}, PO_4^{3-}, CrO_4^{2-}, $Cr_2O_7^{2-}$, MnO_4^{-}, I^{-}, CO_3^{2-}, HCO_3^{-}, $C_2O_4^{2-}$) in 5 mM Tris-HCl/NaCl buffer (pH 7.0). [Zn-CP] = 10 μM and [ions] = 50 μM. λ_{ex}: 312 nm, λ_{F}: 395 nm, slit width: 4 nm.

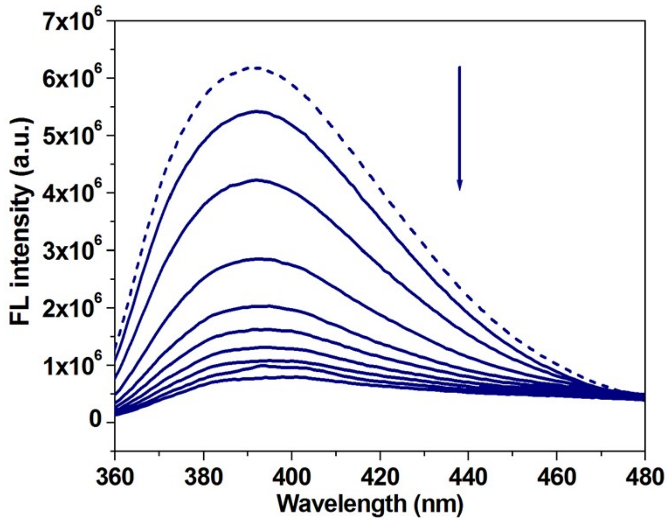

Fig. S11 Luminescence quenching of Tb^{3+}@Zn-CP in 5 mM Tris-HCl/NaCl buffer (pH 7.0) with gradual addition of 1 mM solution of Fe^{3+}. λ_{ex}: 330 nm, λ_F: 390 nm, slit width: 4 nm. [Tb^{3+}@Zn-CP] = 10 μM.

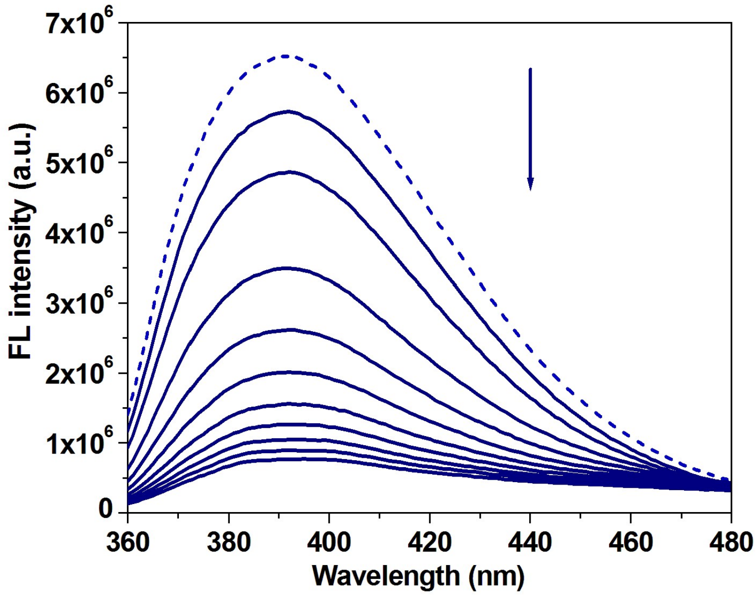

Fig. S12 Luminescence quenching of Tb^{3+}@Zn-CP in 5 mM Tris-HCl/NaCl buffer (pH 7.0) with gradual addition of 1 mM solution of Ru^{3+}. λ_{ex}: 330 nm, λ_F: 390 nm, slit width: 4 nm. [Tb^{3+}@Zn-CP] = 10 μM.

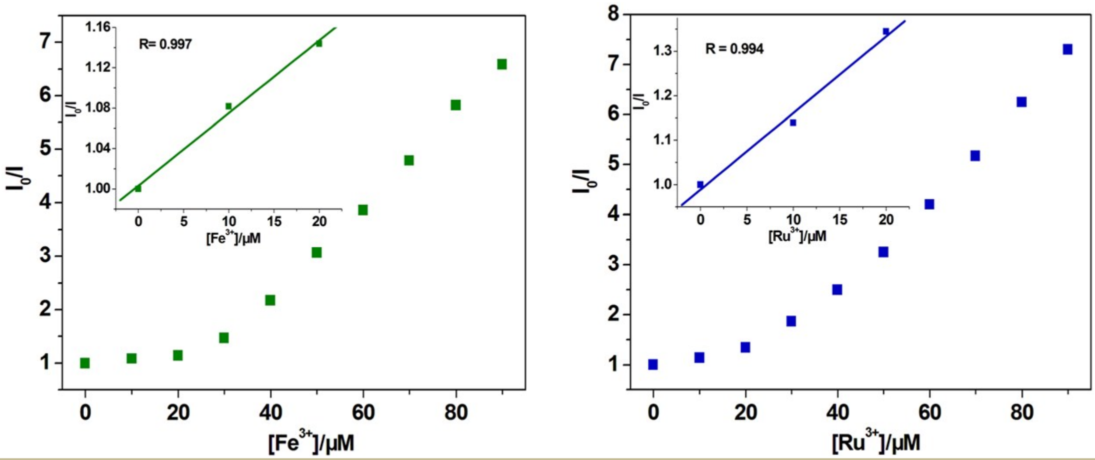

Fig. S13 the Stern−Volmer plots of I_0/I versus $[Fe^{3+}]$ and $[Ru^{3+}]$, respectively (insets: the related Stern−Volmer plots at low $[Fe^{3+}]$ and $[Ru^{3+}]$. λ_{ex}: 330 nm, λ_F: 390 nm, slit width: 4 nm. $[Tb^{3+}@Zn\text{-}CP]$ = 10 μM.

Table S4. Comparison of the probes with literature reports for sensing Fe^{3+}, Ru^{3+}.

S. No	Probe	LOD (M)	Ref
1	$\{[Cd(L)\text{-}(BPDC)]\cdot 2H_2O\}n$ probe $\{[Cd(L)(SDBA)(H_2O)]\cdot 0.5H_2O\}n$ probe	2.21×10^{-6} for Fe^{3+} 7.14×10^{-6} for Fe^{3+}	S1
2	Zn-L-MOF probe	6.4×10^{-6} for Fe^{3+}	S2
3	Zn(II)-based MOF probe	2×10^{-6} for Fe^{3+}	S3
4	Ru probe	5.03 nm means 0.51 ppb for Ru^{3+}	S4
5	Europium-Based MOF probe	0.793×10^{-6} for Fe^{3+}	S5
6	$\{[Eu(Hdcppa)(H_2O)_2]\cdot H_2O\}n$ probe	10^{-6} for Fe^{3+}	S6
7	$Tb^{3+}@Cd\text{-}P$ probe	6.6×10^{-7} for Fe^{3+}	S7
8	Cd-P probe	4.7×10^{-8} for Fe^{3+}	S7
9	$[Zn(modbc)_2]n$	0.57×10^{-6} for Fe^{3+}	This work
10	$[Zn(modbc)_2]n$	0.27×10^{-6} for Ru^{3+}	This work

S1. S. G. Chen, Z. Z. Shi, L. Qin, H. L. Jia, H. G. Zheng, Two New Luminescent Cd(II)-Metal−Organic Frameworks as Bifunctional Chemosensors for Detection of Cations Fe^{3+}, Anions CrO_4^{2-}, and $Cr_2O_7^{2-}$ in Aqueous Solution, *Cryst. Growth Des*. 2017, **17**, 67−72.

S2. Yu, C. Y.; Sun, X. D.; Zou, L. F.; Li, G. H.; Zhang, L. R.; Liu, Y. L. A Pillar-Layered Zn-LMOF with Uncoordinated Carboxylic Acid Sites: High Performance for Luminescence Sensing Fe^{3+} and TNP. *Inorg. Chem*.

2019, *58*, 4026−4032.

S3. Lv, R.; Li, H.; Su, J.; Fu, X.; Yang, B. Y.; Gu, W.; Liu, X. Zinc Metal−Organic Framework for Selective Detection and Differentiation of Fe(III) and Cr(VI) Ions in Aqueous Solution. *Inorg. Chem*. **2017**, *56*, 12348−12356.

S4. B. Chen, F. L. Song, S. G. Sun, J. L.i Fan, X. J. Peng, A Highly Sensitive Fluorescent Chemosensor for Ruthenium: Oxidation Plays a Triple Role, *Chem. Eur. J.* 2013, **19**, 10115–10118.

S5. Purna, C. R.; Mandal, S. Europium-Based Metal−Organic Framework as a Dual Luminescence Sensor for the Selective Detection of the Phosphate Anion and Fe^{3+} Ion in Aqueous Media. *Inorg. Chem*. **2018**, *57*, 11855−11858

S6. Zhang, H. J.; Fan, R. Q.; Chen, W.; Fan, J. Z.; Dong, Y. W.; Song, Y.; Du, X.; Wang, P.; Yang, Y. L. 3D Lanthanide Metal−Organic Frameworks Based on Mono-, Tri-, and Heterometallic Tetranuclear Clusters as Highly Selective and Sensitive Luminescent Sensor for Fe^{3+} and Cu^{2+} Ions. *Cryst. Growth Des*. **2016**, *16*, 5429−5440.

S7 Y. D. Wu, M. H. Lin, D. Y. Liu, M. Liu, J. Qian, Two-dimensional Cd(II) coordination polymer encapsulated by Tb^{3+} as a reversible luminescent probe for Fe^{3+}. *RSC Adv*., **2019**, *9*, 34949–34957.

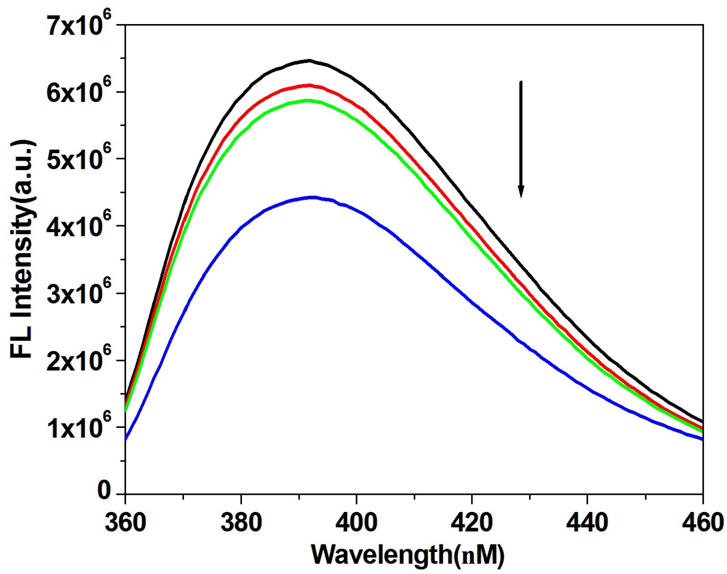

Fig. S14 The relative fluorescence intensity of a 10 μM solution of Tb^{3+}@ Zn-CP upon addition of 1.0 and 9.0 equiv of Fe^{3+} in the presence of 9.0 equiv of background ions (M^{n+}). λ_{ex}: 330 nm, λ_F: 390 nm, slit width: 4 nm.

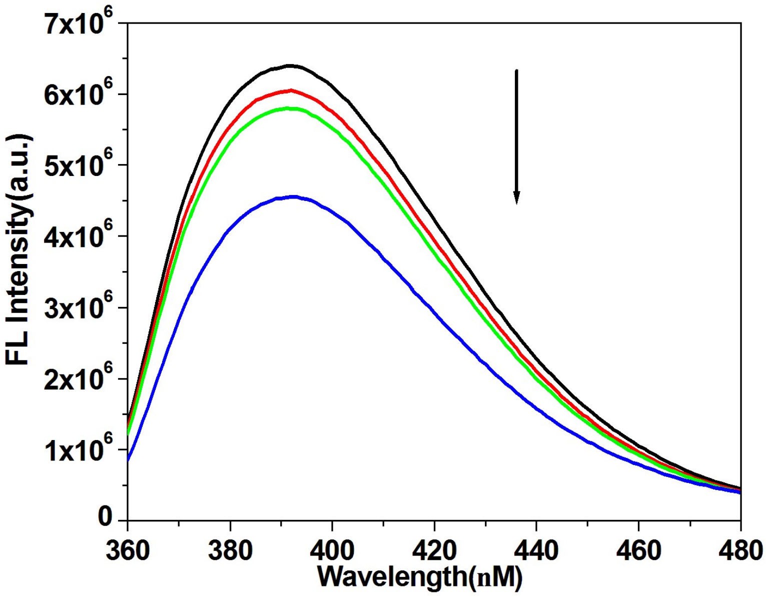

Fig. S15 The relative fluorescence intensity of a 10 μM solution of Tb^{3+}@ Zn-CP upon addition of 1.0 and 9.0 equiv of Ru^{3+} in the presence of 9.0 equiv of background ions (M^{n+}). λ_{ex}: 330 nm, λ_F: 390 nm, slit width: 4 nm.

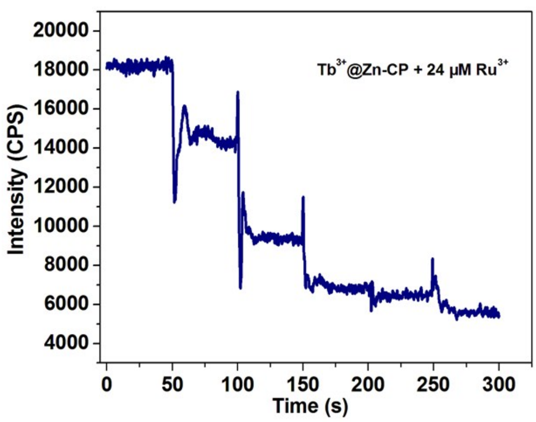

(a)

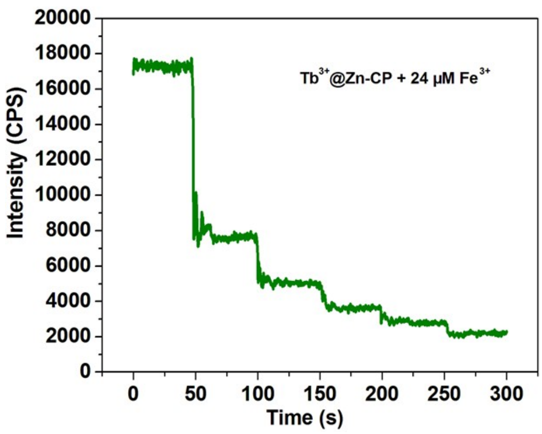

(b)

Fig. S16 The variation of luminescent intensity of Tb^{3+}@ Zn-CP at 390 nm with immersion time in 24 μM $RuCl_3$ aqueous solution (blue, a); with immersion time in 24 μM $Fe(NO_3)_3$ aqueous solution (olive, b).

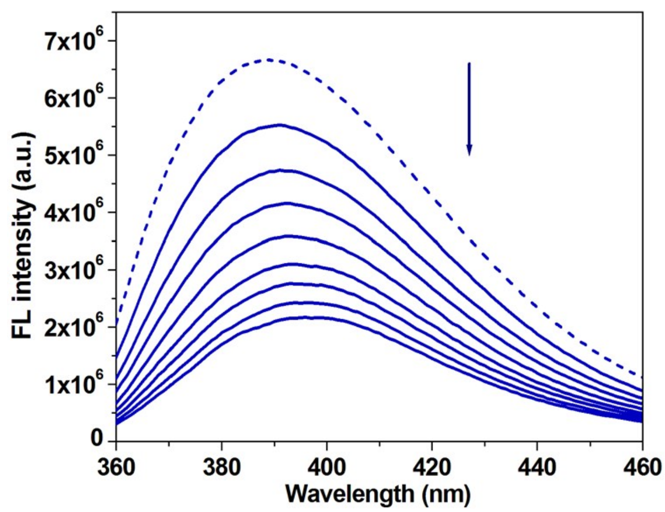

Fig. S17 Luminescence quenching of Tb^{3+}@Zn-CP in 5 mM Tris-HCl/NaCl buffer (pH 6.0) with gradual addition of 1 mM solution of $Cr_2O_7^{2-}$. λ_{ex}: 330 nm, λ_F: 390 nm, slit width: 4 nm. [Tb^{3+}@Zn-CP] = 10 μM.

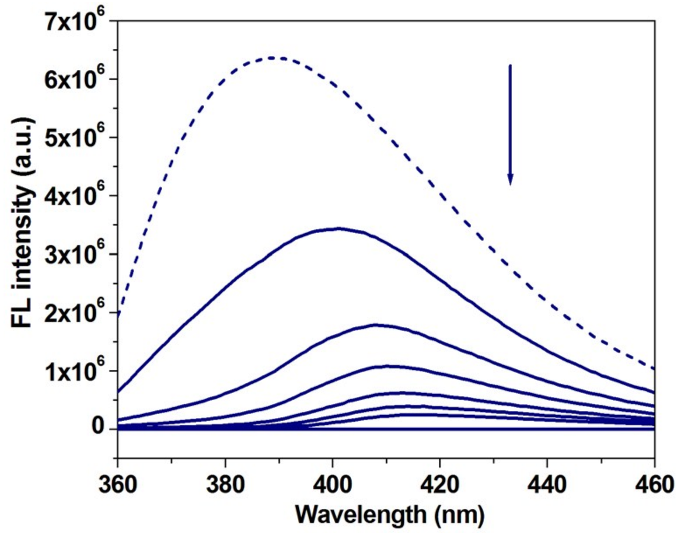

Fig. S18 Luminescence quenching of Tb^{3+}@Zn-CP in 5 mM Tris-HCl/NaCl buffer (pH 8.0) with gradual addition of 1 mM solution of CrO_4^{2-}. λ_{ex}: 330 nm, λ_F: 390 nm, slit width: 4 nm. [Tb^{3+}@Zn-CP] = 10 μM.

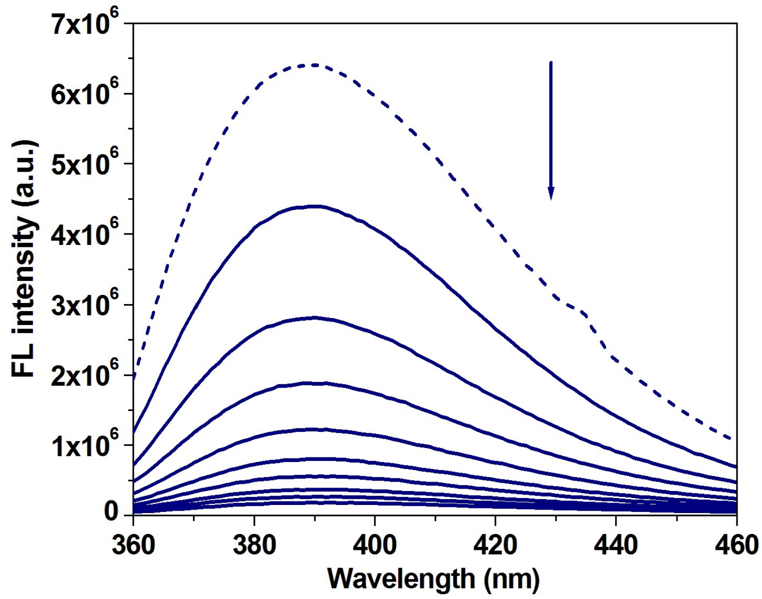

Fig. S19 Luminescence quenching of Tb^{3+}@Zn-CP in 5 mM Tris-HCl/NaCl buffer (pH 7.0) with gradual addition of 1 mM solution of MnO_4^-. λ_{ex}: 330 nm, λ_F: 390 nm, slit width: 4 nm. [Tb^{3+}@Zn-CP] = 10 μM.

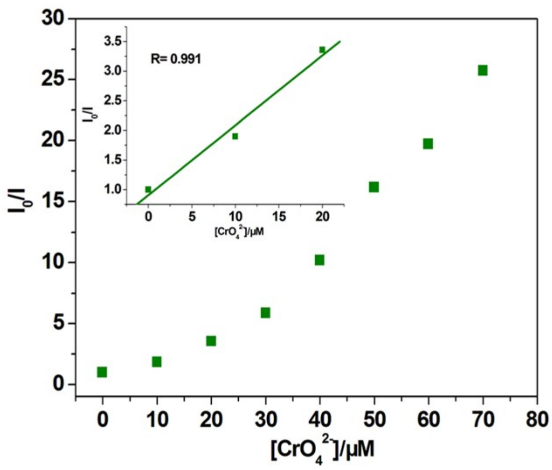

(a)

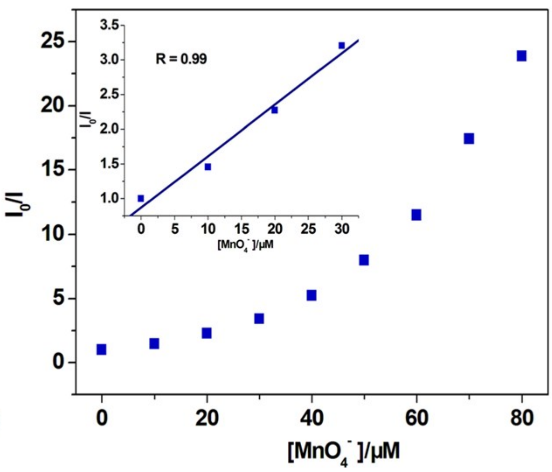

(b)

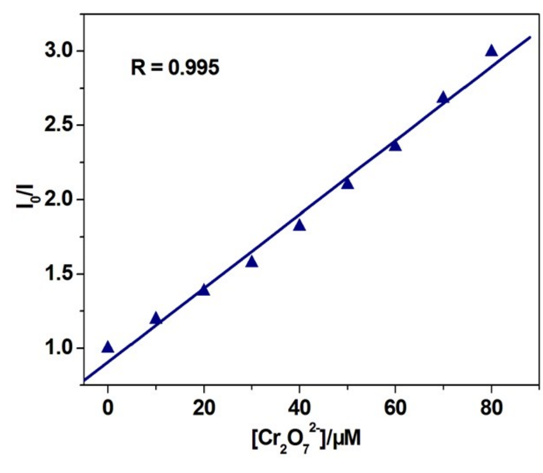

(c)

Fig. S20 the Stern−Volmer plots of I_0/I versus $Cr_2O_7^{2-}$, CrO_4^{2-} and MnO_4^- ion concentrations, respectively (insets: the related Stern−Volmer plots at low [$Cr_2O_7^{2-}$], [CrO_4^{2-}] and [MnO_4^-]. λ_{ex}: 330 nm, λ_F: 390 nm, slit width: 4 nm. [Tb^{3+}@Zn-CP] = 10 μM.

Table S5. Comparison of the probes with literature reports for sensing $Cr_2O_7^{2-}$, CrO_4^{2-} and MnO_4^-.

S. No	Probe	LOD	Ref
1	$[H_2N(CH_3)_2]_2[Zn_2L(HPO_3)_2]$ probe	1.09×10^{-6} M for $Cr_2O_7^{2-}$	S1
2	$\{[Cd(L)\text{-}(BPDC)]\cdot 2H_2O\}n$ probe $\{[Cd(L)(SDBA)(H_2O)]\cdot 0.5H_2O\}n$ probe	3.76×10^{-5} M for $Cr_2O_7^{2-}$ 4.86×10^{-5} M for CrO_4^{2-}	S2
3	$[Cd_3\{Ir(ppy\text{-}COO)_3\}_2(DMF)_2(H_2O)_4]\cdot 6 H_2O\cdot 2DMF$ probe	145.1 ppb for $Cr_2O_7^{2-}$	S3
4	$[Tb_2Ni_3(HCAM)_6(H_2O)_{12}]$ n probe	0.29×10^{-6} M for MnO_4^-	S4
5	$\{[Ba_3La_{0.5}(\mu_3\text{-}L)_{2.5}(H_2O)_3(DMF)]\cdot(3DMF)\}$ n probe	0.28×10^{-6} M for MnO_4^-	S5
6	$[Zn(modbc)_2]n$	0.43×10^{-6} M for $Cr_2O_7^{2-}$	This work
7	$[Zn(modbc)_2]n$	0.10×10^{-6} M for CrO_4^{2-}	This work
8	$[Zn(modbc)_2]n$	0.15×10^{-6} M for MnO_4^-	This work

S1. Si-Fu Tang , Xiaomin Hou, A Highly Stable Dual Functional Zinc Phosphite Carboxylate as Luminescent Sensor of Fe^{3+} and $Cr_2O_7^{2-}$, *Cryst. Growth Des*. 2019, **19**, 45−48.

S2. S. G. Chen, Z. Z. Shi, L. Qin, H. L. Jia, H. G. Zheng, Two New Luminescent Cd(II)-Metal−Organic Frameworks as Bifunctional Chemosensors for Detection of Cations Fe^{3+}, Anions CrO_4^{2-}, and $Cr_2O_7^{2-}$ in Aqueous Solution, *Cryst. Growth Des*. 2017, **17**, 67−72.

S3. Kun Fan, Song-Song Bao, Wei-Xuan Nie, Chwen-Haw Liao, and Li-Min Zheng, Iridium(III)-Based Metal−Organic Frameworks as Multiresponsive Luminescent Sensors for Fe^{3+}, $Cr_2O_7^{2-}$, and ATP^{2-} in Aqueous Media, Inorg. Chem. 2018, 57, 1079−1089.

S4. Jing Qian, Mei-Mei Sun, Ming Liu, Wen Gu, Macromolecular Probe Based on a Ni II /Tb III Coordination Polymer for Sensitive Recognition of Human Serum Albumin (HSA) and MnO_4^-, ACS Omega 2019, 4, 11949−11959.

S5. Ding, B.; Liu, S. X.; Cheng, Y.; Guo, C.; Wu, X. X.; Guo, J. H.; Liu, Y. Y.; Li, Y. Heterometallic Alkaline Earth-Lanthanide Ba(II)-La(III) Microporous Metal-Organic Framework as Bifunctional Luminescent Probes of

Al $^{3+}$ and MnO_4^-. Inorg. Chem. 2016, 55, 4391−4402.

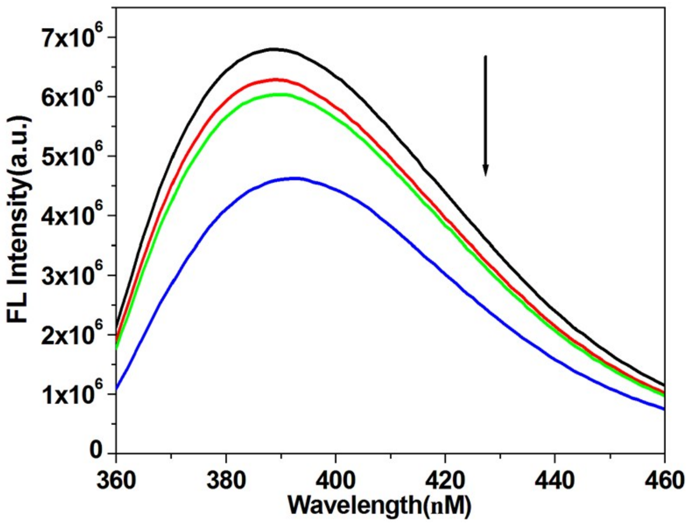

Fig. S21 The relative fluorescence intensity of a 10 μM solution of Tb^{3+}@ Zn-CP upon addition of 1.0 and 6.0 equiv of $Cr_2O_7^{2-}$ in the presence of 6.0 equiv of background ions (M^{n+}). λ_{ex}: 330 nm, λ_F: 390 nm, slit width: 4 nm.

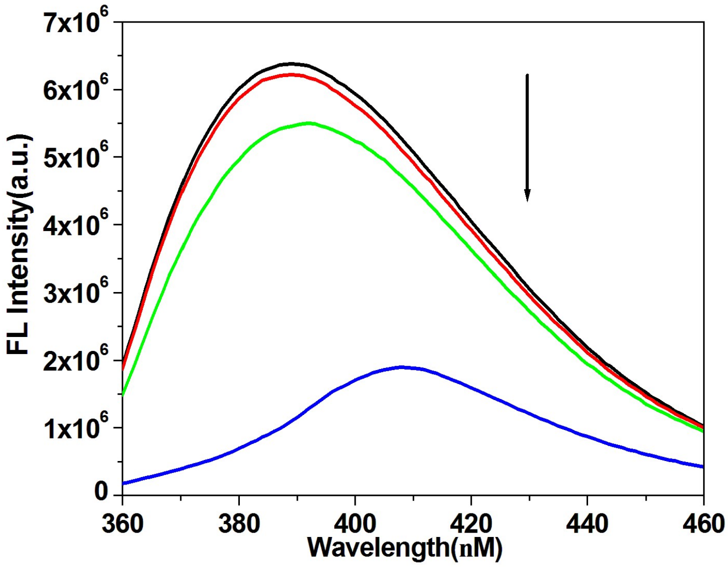

Fig. S22 The relative fluorescence intensity of a 10 μM solution of Tb^{3+}@ Zn-CP upon addition of 1.0 and 6.0 equiv of CrO_4^{2-} in the presence of 6.0 equiv of background ions (M^{n+}). λ_{ex}: 330 nm, λ_F: 390 nm, slit width: 4 nm.

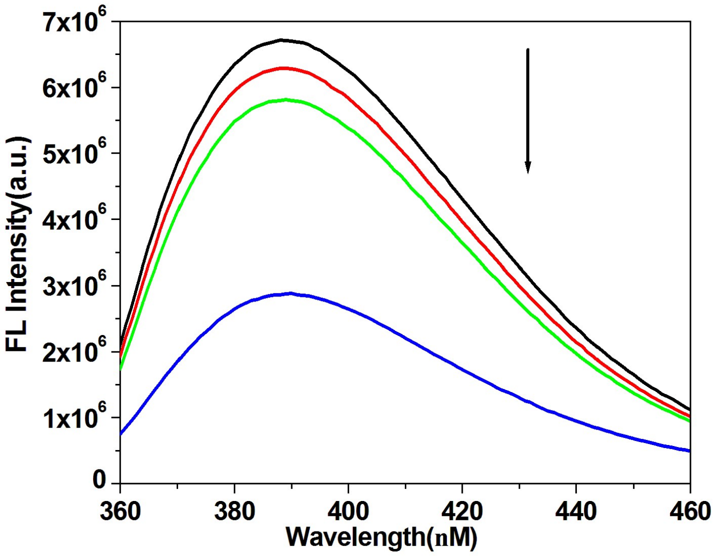

Fig. S23 The relative fluorescence intensity of a 10 μM solution of Tb^{3+}@ Zn-CP upon addition of 1.0 and 6.0 equiv of MnO_4^- in the presence of 6.0 equiv of background ions (M^{n+}). λ_{ex}: 330 nm, λ_F: 390 nm, slit width: 4 nm.

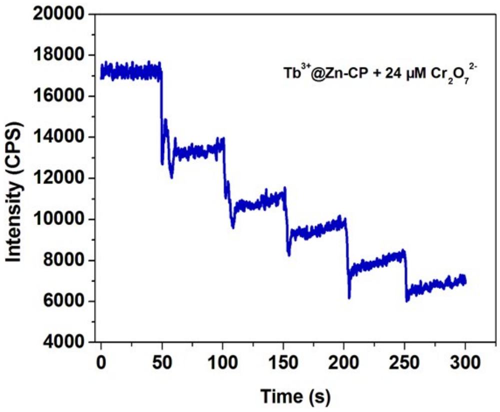

(a)

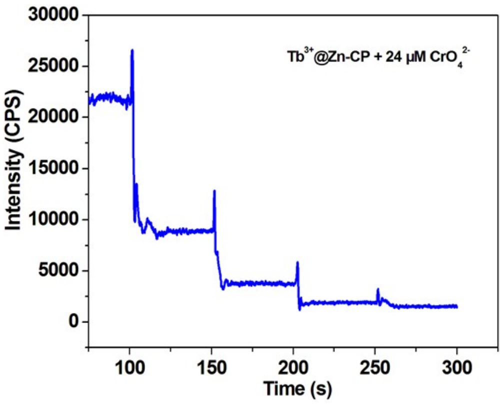

(b)

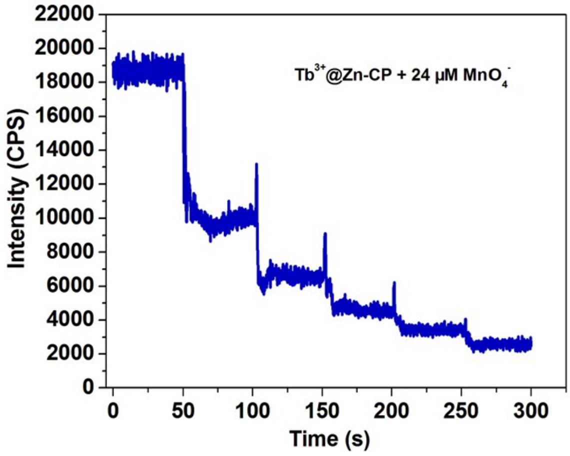

(c)

Fig. S24 The variation of luminescent intensity of Tb^{3+}@ Zn-CP at 390 nm with immersion time in 24 μM $Cr_2O_7^{2-}$ aqueous solution (a); with immersion time in 24 μM CrO_4^{2-} aqueous solution (b); with immersion time in 24 μM MnO_4^- aqueous solution (c).

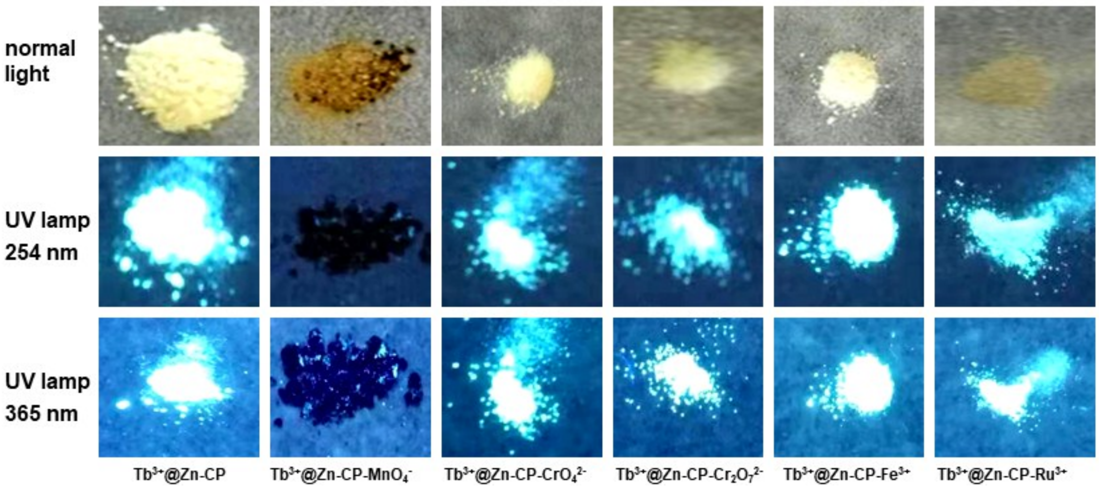

Fig. S25 Color of Tb^{3+}@Zn-CP dipped in $KMnO_4$, K_2CrO_4, $K_2Cr_2O_7$, $FeCl_3$, $RuCl_3$ solution by normal light and UV lamp.

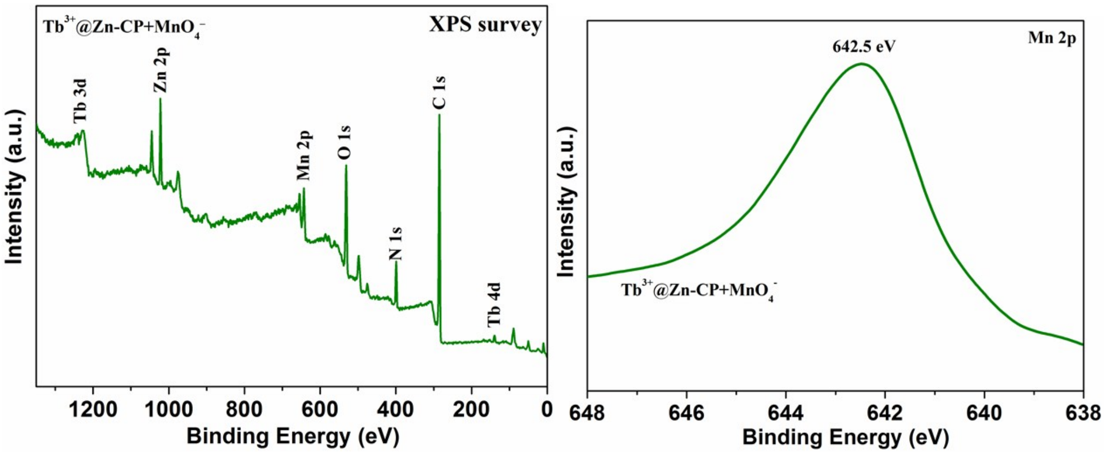

Fig. S26 The XPS spectra of Tb^{3+}@Zn-CP+MnO_4^- samples: the survey spectrum and the high resolution XPS spectra of Mn 2p.

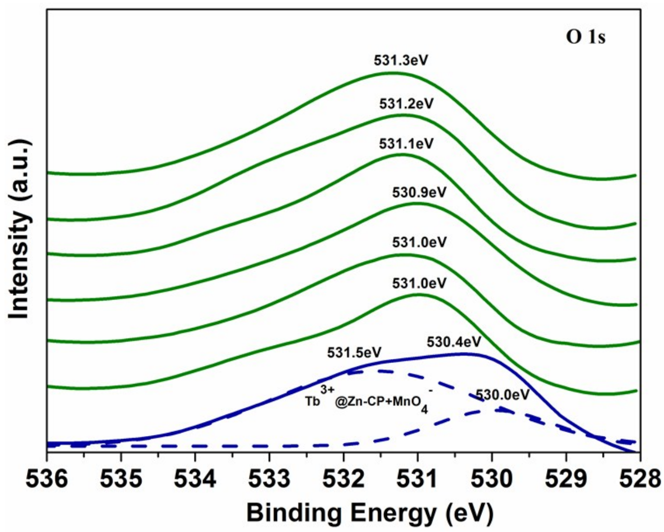

Fig. S27 The high resolution XPS spectra of O 1s of Zn-CP, Tb^{3+}@Zn-CP, Tb^{3+}@Zn-CP+Ru^{3+}, Tb^{3+}@Zn-CP+Fe^{3+}, Tb^{3+}@Zn-CP+$Cr_2O_7^{2-}$, Tb^{3+}@Zn-CP+CrO_4^{2-} and Tb^{3+}@Zn-CP+MnO_4^- samples.

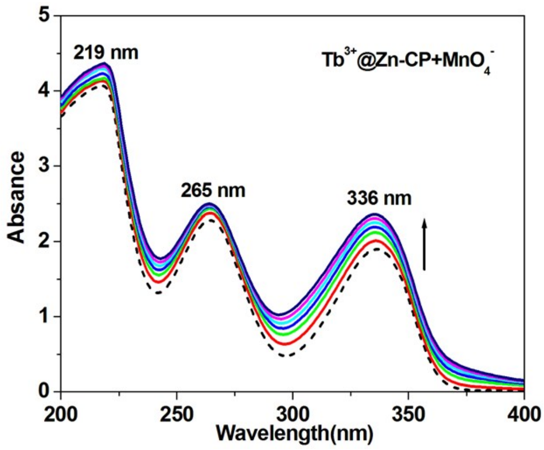

Fig. S28 UV–vis absorption spectra of Tb^{3+}@Zn-CP with different concentration of MnO_4^-. Solvent: DMF/H_2O (3/1, v/v), c: 10 μM for Tb^{3+}@Zn-CP, from bottom to top, the equiv of MnO_4^-: 0, 5, 10, 15, 20, 25, 30.

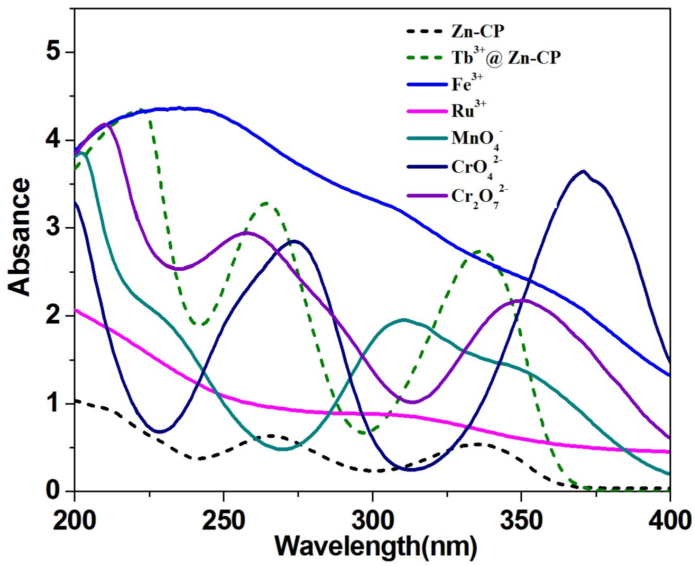

Fig. S29 UV spectra of Fe^{3+}, Ru^{3+}, CrO_4^{2-}, $Cr_2O_7^{2-}$, MnO_4^- in H_2O; and Zn-CP, Tb^{3+}@Zn-CP in DMF.

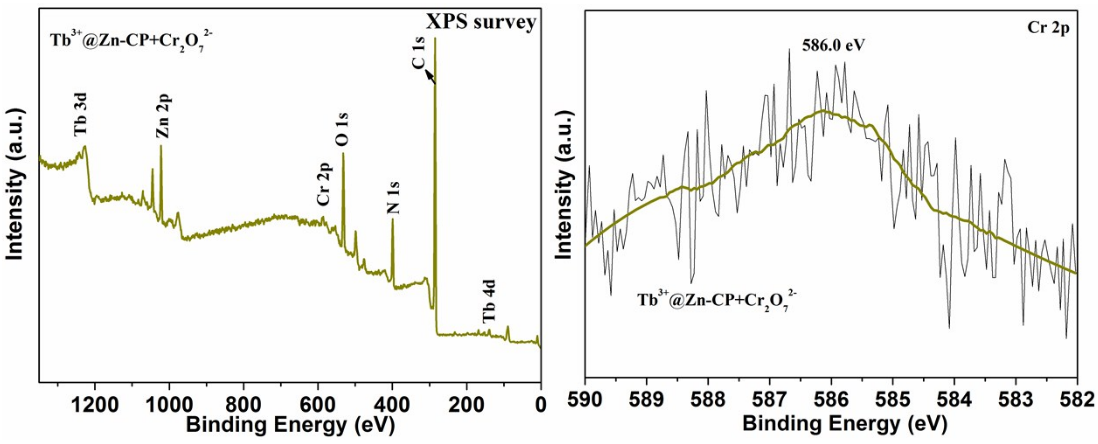

Fig. S30 The XPS spectra of Tb^{3+}@Zn-CP+ $Cr_2O_7^{2-}$ samples: the survey spectrum and the high resolution XPS spectra of Cr 2p.

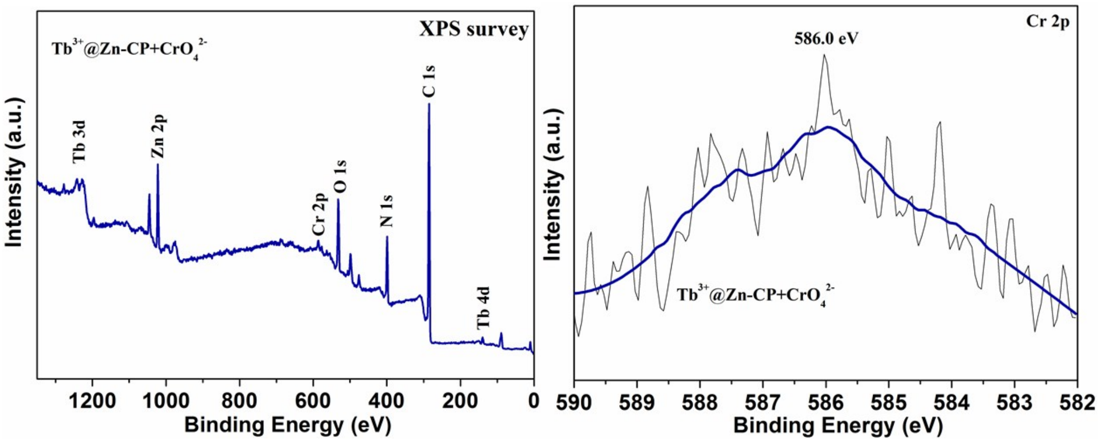

Fig. S31 The XPS spectra of Tb^{3+}@Zn-CP+ CrO_4^{2-} samples: the survey spectrum and the high resolution XPS spectra of Cr 2p.

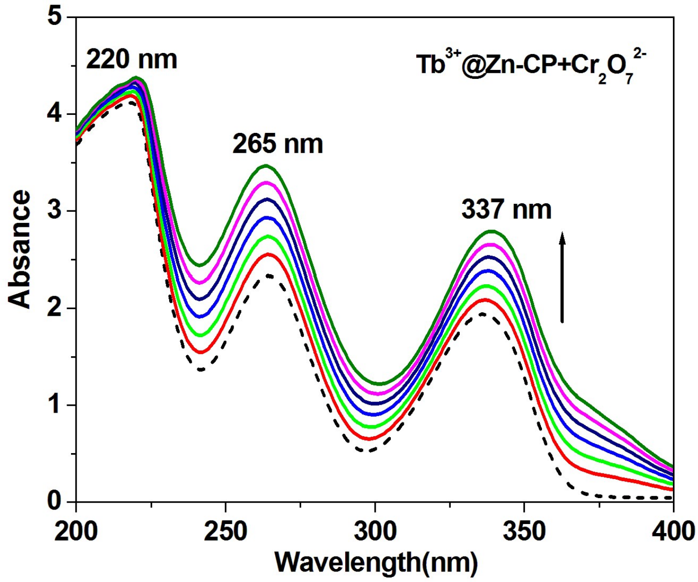

Fig. S32 UV–vis absorption spectra of Tb^{3+}@Zn-CP with different concentration of $Cr_2O_7^{2-}$. Solvent: DMF/H_2O (3/1, v/v), c: 10 μM for Tb^{3+}@Zn-CP, from bottom to top, the equiv of $Cr_2O_7^{2-}$: 0, 5, 10, 15, 20, 25, 30.

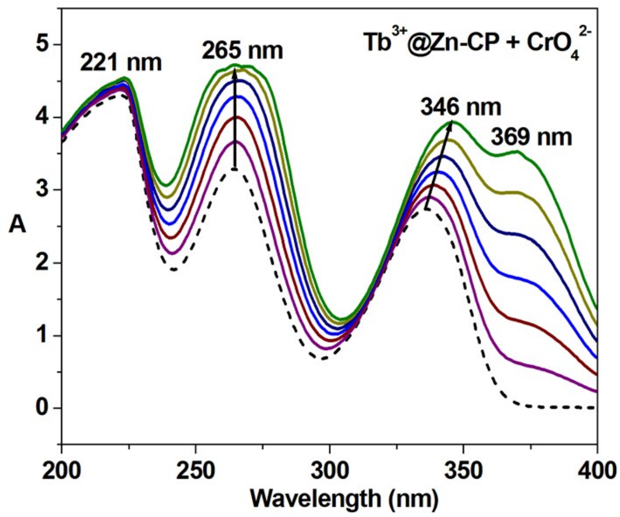

Fig. S33 UV–vis absorption spectra of Tb^{3+}@Zn-CP with different concentration of CrO_4^{2-}. Solvent: DMF/H_2O (3/1, v/v), c: 10 μM for Tb^{3+}@Zn-CP, from bottom to top, the equiv of CrO_4^{2-}: 0, 1, 2, 3, 4, 5, 6.

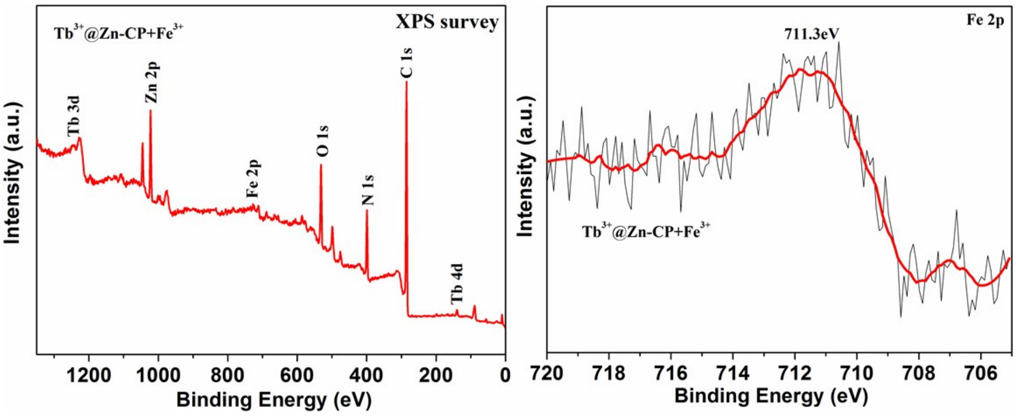

Fig. S34 The XPS spectra of Tb^{3+}@Zn-CP+Fe^{3+} samples: the survey spectrum and the high resolution XPS spectra of Fe 2p.

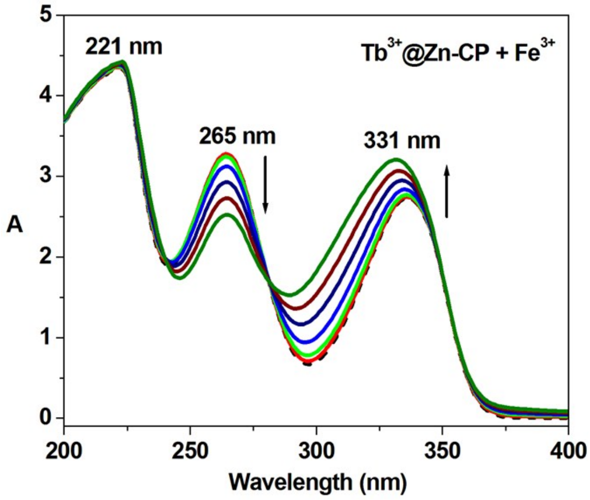

Fig. S35 UV–vis absorption spectra of Tb^{3+}@Zn-CP with different concentration of Fe^{3+}. Solvent: DMF/H_2O (3/1, v/v), c: 10 μM for Tb^{3+}@Zn-CP, from bottom to top, the equiv of Fe^{3+}: 0, 1, 2, 3, 4, 5,6.

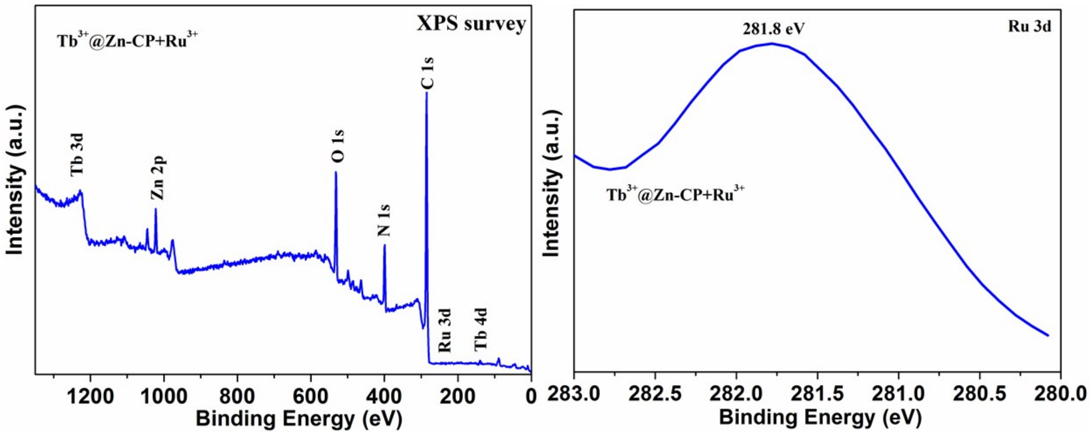

Fig. S36 The XPS spectra of Tb^{3+}@Zn-CP+Ru^{3+} samples: the survey spectrum and the high resolution XPS spectra of Ru 3d.

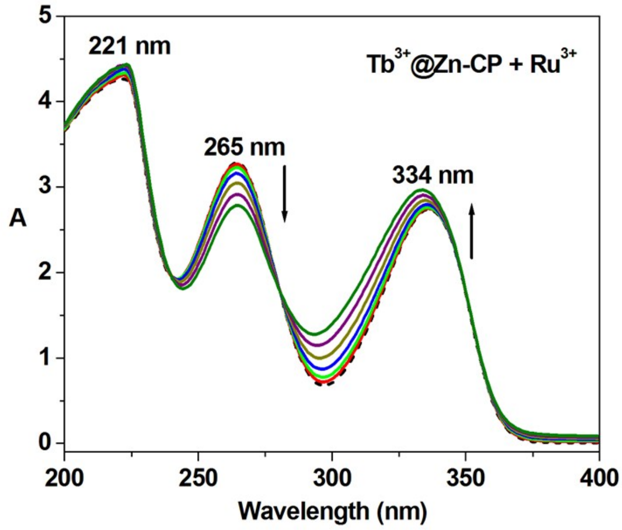

Fig. S37 UV–vis absorption spectra of Tb^{3+}@Zn-CP with different concentration of Ru^{3+}. Solvent: DMF/H_2O (3/1, v/v), c: 10 μM for Tb^{3+}@Zn-CP, from bottom to top, the equiv of Ru^{3+}: 0, 1, 2, 3, 4, 5, 6.

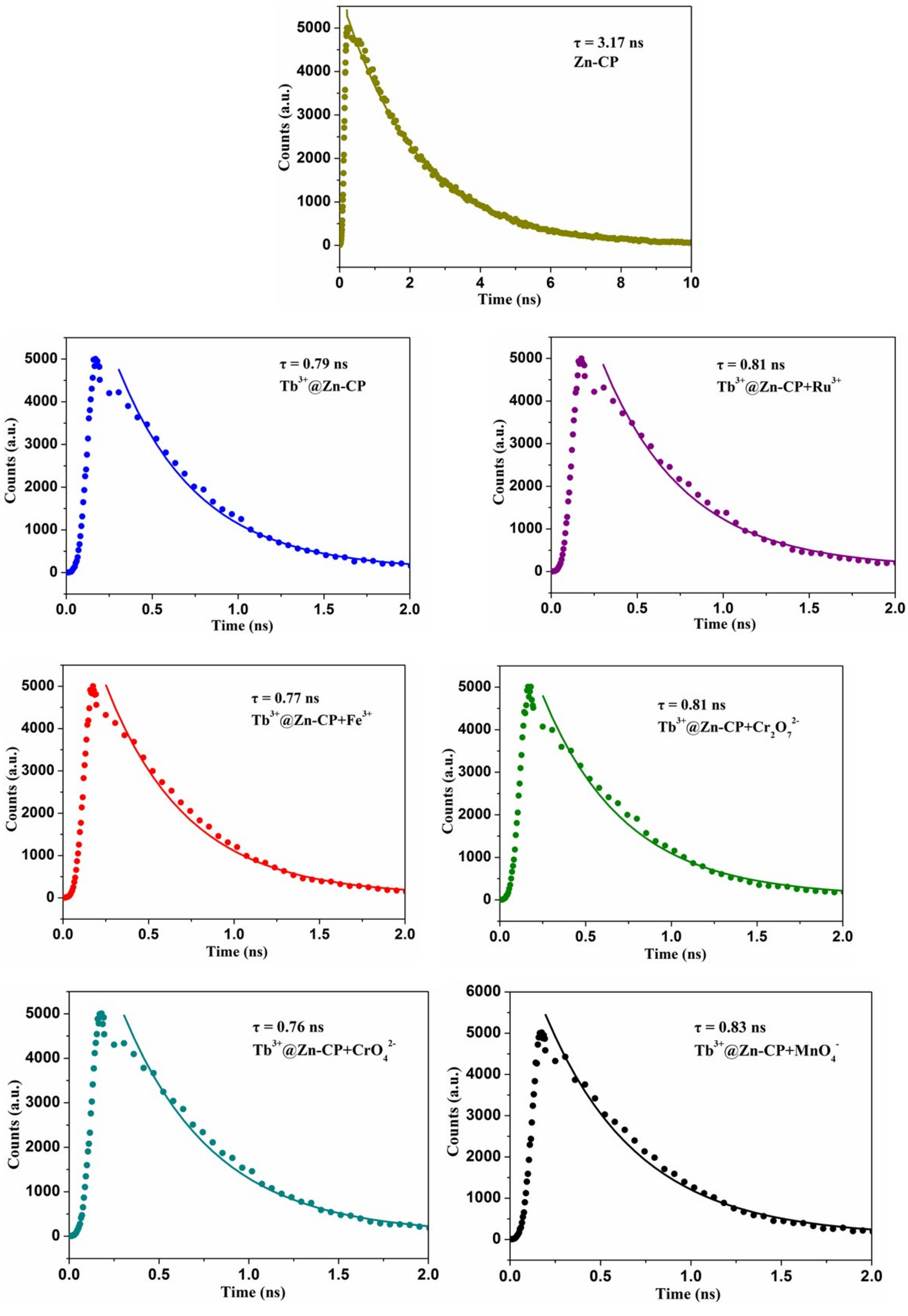

Fig. S38 Temporal fluorescence decay of 10 μM Zn-CP with 50 μM Fe^{3+}, Ru^{3+}, CrO_4^{2-}, $Cr_2O_7^{2-}$, MnO_4^- in 5 mM Tris-HCl/NaCl buffer (pH 7.0) excited at 330 nm and monitored at 390 nm; The data are obtained at 54.9 ps per point.

Table S6 Comparison of lifetimes of Tb^{3+}@Zn-CP, Tb^{3+}@Zn-CP+Fe^{3+}, Tb^{3+}@Zn-CP+Ru^{3+},

Tb^{3+}@Zn-CP+$Cr_2O_7^{2-}$, Tb^{3+}@Zn-CP+CrO_4^{2-} and Tb^{3+}@Zn-CP+MnO_4^-.

Compounds	τ_1(ns)	B_1(%)	τ_2(ns)	B_2(%)	τ(ns)
Zn-CP	47.28	2.25	2.15	97.75	3.17
Tb^{3+}@Zn-CP	0.51	88.21	2.87	11.79	0.79
Tb^{3+}@Zn-CP+Fe^{3+}	0.48	87.09	2.69	12.91	0.77
Tb^{3+}@Zn-CP+Ru^{3+}	0.46	84.49	2.69	15.51	0.81
Tb^{3+}@Zn-CP+MnO_4^-	0.48	84.76	2.76	15.24	0.83
Tb^{3+}@Zn-CP+CrO_4^{2-}	2.86	10.91	0.50	89.09	0.76
Tb^{3+}@Zn-CP+$Cr_2O_7^{2-}$	0.48	84.58	2.59	15.42	0.81